

## EFFECTS OF GRAVITATIONAL EVOLUTION, BIASING, AND REDSHIFT SPACE DISTORTION ON TOPOLOGY

CHANGBOM PARK, JUHAN KIM

Korea Institute for Advanced Study, Dongdaemun-gu, Seoul 207-43, Korea

AND

J. RICHARD GOTT III

Department of Astrophysical Sciences, Peyton Hall, Princeton University, Princeton, NJ 08544, USA

*Not to appear in Nonlearned J., 45.*

### ABSTRACT

We have studied the dependence of topology of large scale structure on tracer, gravitational evolution, redshift space distortion, and cosmology. A series of large N-body simulations of the  $\Lambda$ CDM and SCDM models that have evolved 1.1 or 8.6 billion particles, are used in the study. Evolution of the genus statistic, used as a topology measure, from redshift 8 to 0 is accurately calculated over a wide range of smoothing scales using the simulations. The tracers of large scale structure considered are the CDM matter, biased peaks in the initial density field, dark halos, and ‘galaxies’ populating the dark halos in accordance with a Halo Occupation Distribution (HOD) model.

We have found that the effects of biasing, gravitational evolution, and initial conditions on topology of large scale structure are all comparable. The redshift space distortion effects are relatively small down to about  $5 h^{-1}\text{Mpc}$  for all tracers except for the high threshold part of the genus curve. The gravitational effects are found to be well-modeled by the analytic perturbation theory when the CDM matter distribution is considered. But the direction of gravitational evolution of topology can be even reversed for different tracers. For example, the shift parameter of the genus curve evolves in opposite directions for matter and HOD ‘galaxies’ at large scales. At small scales there are interesting deviations of the genus curve of dark halos and ‘galaxies’ from that of matter in our initially Gaussian simulations. The deviations should be understood as due to combined effects of gravitational evolution and biasing. This fact gives us an important opportunity: topology of large scale structure can be used as a strong constraint on galaxy formation mechanisms. At scales larger than  $20 h^{-1}\text{Mpc}$  all the above effects gradually decrease. With a good knowledge of the effects of non-linear gravitational evolution and galaxy biasing on topology one can also constrain the Gaussian random phase initial conditions hypothesis to high accuracy.

*Subject headings:*

### 1. INTRODUCTION

Topology analysis has long been applied to galaxy redshift survey data to test one of the major predictions of simple inflationary scenarios: that the primordial density fluctuations are Gaussian random phase (Gott, Melott, & Dickinson 1986; Gott et al. 1989; Vogeley et al. 1994). To recover the primordial density fluctuations it is necessary to smooth the observed sample over large enough scales to reach the linear regime. Since redshift surveys have not been very deep in the past, one was left with a small dynamic range for topology study after big smoothings, and it has been hard to draw firm conclusions on the nature of the initial density field. As ambitious new redshift surveys like the 2dF and the Sloan Digital Sky Surveys (<http://sdss.org>) are being completed, it is now hoped that the topology analysis can become one of the precision measures for cosmology. These surveys are not just large in angle and deep in depth, but are also dense. This means that the new survey samples can be used to study the primordial density field at large scales, and also to explore small-scale phenomena like the formation of galaxies.

Since the main purpose of studying topology has been to discover the Gaussianity of the linear density field, there has been relatively little work on topology at small

non-linear scales. One work on small scale topology is Springel et al. (1998) who applied the analysis to their N-body simulations and the 1.2-Jy IRAS galaxy sample. However, without quantitatively studying the complete scale- and cosmology dependences of topology, as measured by the genus, they have incorrectly concluded that the shape of the genus curve is that of a random phase field far into the non-linear regime, and that the amplitude drop of the genus curve due to the phase correlation is the only sensitive measure of non-linearity. In this paper we will show that topology analysis becomes useful when a sample is studied over a wide range of smoothing scale and when quantitative measures of the deviation of the genus curve from the Gaussian one are used. In particular, we will present our finding that topology of underdense regions at small scales is sensitive to the structure formation mechanism. This fact opens the possibility that galaxy formation can be better understood by studying the small scale topology of galaxy distribution.

Previous analyses of observational samples for topology study have generally used the dark matter distribution for comparison. The similarity of the observed genus curves to those obtained from simulated matter distribution has been investigated for various cosmologies. This may be fine when the uncertainties in genus

measured from observations are much larger than the effects of biasing and redshift space distortion. With the unprecedented accuracy provided by observational data like the SDSS sample, however, these effects have to be accurately accounted for. In this paper we will study the gravitational evolution of the genus of peaks in the initial density field and dark halos as well as dark matter to see the dependence of topology on these tracers. Redshift space distortion effects are also studied. They all have non-negligible, important effects on the genus curve.

Our work is numerical since the main purposes of our work is to explore the strong non-linear effects of gravitational evolution through topology analysis where current analytic approaches are inadequate. Study of the tracer dependence of, and biasing effects on, topology also requires numerical simulations. To check for the important question of whether the topology is consistent with Gaussian random phase initial conditions to high accuracy in the new large observational data sets given that the effects of non-linear evolution and biasing are detectable in such surveys, the best method would seem to be direct comparison with large cosmological simulations with Gaussian random phase initial conditions where non-linear evolution and biasing are properly modeled. If agreement is obtained, this supports the Gaussian random phase initial conditions hypothesis to high accuracy.

Introduction to the genus and its related statistics is given in sections 2 and 3. Our N-body simulations used in this study are described in section 4. Evolution of the genus curve is studied in section 5 for matter and ‘galaxy’ distributions in the  $\Lambda$ CDM and SCDM cosmologies. Conclusions follow in section 6.

## 2. GENUS

To measure topology of a tracer distribution we calculate the genus of iso-density surfaces as a function of density threshold level. The genus is defined as

$$G = \text{Number of holes in contour surfaces} \\ - \text{Number of isolated regions} \quad (1)$$

in the isodensity surfaces at a given threshold level. In this definition, a sphere has genus of  $-1$ , and a torus has genus  $0$  (Gott, Melott & Dickinson 1986). The Gauss-Bonnet theorem connects the global topology with an integral of local curvature of the surface  $S$ , i.e.

$$G = -\frac{1}{4\pi} \int_S \kappa dA, \quad (2)$$

where  $\kappa$  is the local Gaussian curvature. The genus is equal to  $-1/2$  times the Euler characteristic, or the fourth Minkowski Functional in 3-dimensions (Mecke, Buchert, & Wagner 1994; Schmalzing & Buchert 1997).

For a Gaussian random field an analytic formula exists for the genus-threshold density relation (Hamilton, Gott, & Weinberg 1986). The genus per unit volume is

$$g(\nu) = A(1 - \nu^2)e^{-\nu^2/2}, \quad (3)$$

where  $\nu \equiv (\rho - \bar{\rho})/\sigma$  is the threshold density in unit of standard deviations  $\sigma = \langle(\rho - \bar{\rho})^2\rangle^{1/2}$  from the mean. The amplitude is

$$A = \frac{1}{(2\pi)^2} \left(\frac{\langle k^2 \rangle}{3}\right)^{3/2}, \quad (4)$$

where the second moment

$$\langle k^2 \rangle = \int P(k)W(k)k^2 d^3k / \int P(k)W(k)d^3k \quad (5)$$

depends only on the shape of the power spectrum and the smoothing kernel  $W$ . Instead of using  $\nu$  to identify isodensity contours we use the volume fraction label  $\nu_f$  at which the corresponding isodensity contours enclose the fraction of the sample volume equal to that at the density threshold  $\nu_f\sigma$  in the case of a Gaussian field. In this way the genus curve becomes independent of the one-point probability distribution function, which can be better studied by different statistics. Use of  $\nu_f$  also makes the genus curves less sensitive to details of bias (Park & Gott 1991), which is beneficial in studying the primordial field.

## 3. GENUS-RELATED STATISTICS

### 3.1. Shift Parameter

Any departure of the genus curve from the relation given by equation (3) indicates non-Gaussianity of the field. To quantify the deviation we define a set of genus-related statistics. The first statistic  $\Delta\nu$  measures the shift of the middle part of the genus curve. We compute  $\Delta\nu$  defined by (Park et al. 1992)

$$\Delta\nu = \int_{-1}^1 \nu G_{\text{obs}}(\nu) d\nu / \int_{-1}^1 G_{\text{fit}}(\nu) d\nu, \quad (6)$$

where  $G_{\text{obs}}(\nu)$  is the measured genus and  $G_{\text{fit}}(\nu)$  is the random-phase curve best fit to the measured genus data from  $\nu = -1$  to  $+1$ . The best fitting amplitude  $A_{\text{obs}}$  of the observed genus curve is obtained from  $G_{\text{fit}}(0)$ .

### 3.2. Amplitude Drop

The second statistic is the amplitude drop of the genus curve. The density field with phase correlation due to gravitational evolution typically has a fewer number of structures compared to that with the same power spectrum but with random phases. A derived statistic is

$$R_A = A_{\text{obs}}/A_{\text{PS}}, \quad (7)$$

where  $A_{\text{PS}}$  is the amplitude expected for a Gaussian field which has the power spectrum (PS) of the evolved particle/‘galaxy’ distribution. Existence of phase correlation reduces  $R_A$  below 1 (Vogeley et al. 1994; Canavezes et al. 1998). The best fitting amplitude  $A_{\text{obs}}$  is measured as explained above. To calculate  $A_{\text{PS}}$  the PS of the distribution is needed. In this study tracers are contained in simulation cubes with periodic boundaries, and the PS is obtained by Fourier transforming the distribution. Extrapolations of the PS beyond the observed  $k$ -window necessary to calculate the integral for  $A_{\text{PS}}$  introduce only a small error in  $A_{\text{PS}}$  when  $\bar{d}/\sqrt{2} \leq R_G \leq r_{\text{max}}/10$  where  $R_G$  is the Gaussian smoothing length,  $\bar{d}$  is the mean tracer separation, and  $r_{\text{max}}$  is the sample size.

### 3.3. Cluster/Void Abundance Parameters

The third statistic is the numbers of clusters and voids. The statistic  $A_C$  is defined as

$$A_C = \int G_{\text{obs}}(\nu) d\nu / \int G_{\text{fit}}(\nu) d\nu, \quad (8)$$

TABLE 1  
CHARACTERISTICS OF COSMOLOGICAL N-BODY SIMULATIONS

Name	$\Omega_m$	$\Omega_\Lambda$	$h$	$b$	$N_m^a$	$N_p$	$L^b$	$z_i$	$N_{step}$	code
LCDM1024	0.27	0.73	0.71	1.11	$2048^3$	$2048^3$	1024	17	680	PMTree
LCDM5632	0.27	0.73	0.71	1.11	$2048^3$	$2048^3$	5632	17	170	PMTree
LCDM410	0.27	0.73	0.71	1.11	$2048^3$	$1024^3$	409.6	47	470	PM
SCDM1024	1.00	0.00	0.5	1.5	$2048^3$	$1024^3$	1024	23	230	PM
SCDM410	1.00	0.00	0.5	1.5	$2048^3$	$1024^3$	409.6	47	470	PM

<sup>a</sup>Size of mesh on which initial conditions are defined.

<sup>b</sup>( $h^{-1}$ Mpc)

where the integral is limited to  $1.2 \leq \nu \leq 2.2$  which is roughly centered at  $\nu = \sqrt{3}$  which is the minimum in the best fit random phase curve where the number of isolated clusters is greatest.  $A_V$  is similarly defined over  $-2.2 \leq \nu \leq -1.2$  roughly centered at  $\nu = -\sqrt{3}$ , the minimum in the best fit random phase curve where the number of isolated voids is greatest. Here the best-fit Gaussian curve  $G_{\text{fit}}$  is obtained as explained above using the middle part of the genus curve. The statistics  $A_C$  and  $A_V$  quantify the asymmetry of the genus curve and the multiplicity of clusters and voids.

#### 4. SIMULATIONS

In order to study the behaviour of the genus statistic accurately we have made a set of large N-body simulations using a PM and PM+Tree codes. Our PM code uses the triangular-shaped cloud method for mass assignment and force interpolation at particle positions. The force calculation at mesh points is done by the four-point finite difference algorithm (Park 1990, 1997). The PM+Tree code GOTPM, which is a merged version of our PM code with Dubinski’s tree code, is a parallel code which adds the tree force to the PM force at separations shorter than 4 times the pixel size of the mesh used in the PM part (Dubinski et al. 2003). For topology study of the matter distribution, the PM code is preferred since this code can make simulations with large dynamic range in mass at relatively low cost. The PM code is also preferred when the peaks in the initial density field are used as biased tracers because high-resolution initial density fields are adopted in this code. Due to its high force resolution power the PM+Tree code should be the choice when dark halos are targets for topology study. Because a single simulation cannot satisfy all of our needs we have made several simulations supplementing one another using the PM and PM+Tree codes. Parameters of our simulations are summarized in Table 1.

Our results are mainly derived from PM+Tree simulations of the  $\Lambda$ CDM model with the WMAP parameters, namely, the density parameters  $\Omega_m = 0.27$ ,  $\Omega_\Lambda = 0.73$ , the Hubble constant  $h = 0.71$ ,  $\sigma_{m,8} = 0.9$ , and the matter is dominated by the cold dark matter (CDM). Here  $\sigma_{m,8}$  is the RMS mass fluctuation in a sphere of radius of  $8 h^{-1}$  Mpc. The physical sizes of the two simulation cubes are  $L = 1024$  and  $5632h^{-1}$  Mpc. We call them LCDM1024 and LCDM5632. We use the transfer function of the power spectrum given by Bardeen et al. (1986) for LCDM1024. But we have used Eisenstein & Hu (1998)’s power spectrum with  $\Omega_{\text{baryon}} = 0.0463$

for LCDM5632 to include baryonic effects. The number of CDM particles evolved in both simulations is  $2048^3 = 8.59$  billion, among the largest N-Body simulations ever made. A  $2048^3$  mesh is used for the PM part, and the force softening length in the Tree part is one tenth of the mean particle separation. Therefore, the dynamic range in length is  $2 \times 10^4$ , from 0.05 to  $1024 h^{-1}$  Mpc while the dynamic range in mass is  $8.6 \times 10^9$ , from  $9.4 \times 10^9$  to  $8.0 \times 10^{19} h^{-1} M_\odot$  in the case of LCDM1024, for example. Dark halos are identified in the LCDM1024 simulation made by the PM+Tree code. Halo centers are found as local density peaks defined on a fine mesh. The CDM particles belonging to virialized dark halos are searched by checking their binding energy to the local halo centers and tidal radii of subhalos with respect to adjacent bigger halos (Kim & Park 2005). These identification criteria overcome many of the problems and artificial results obtained from existing group-finding algorithms, and let us obtain a catalog of self-bound physical dark halos. Only the dark halos with more than 53 member particles or heavier than  $5 \times 10^{11} h^{-1} M_\odot$  are adopted.

Even though our group finding algorithm allows us to identify many subhalos contained in big halos, those halos with mass much higher than  $10^{13} M_\odot$  cannot be considered to be a single galaxy. On the other hand, every halo identified in the N-body simulation might not contain a galaxy. Therefore, even though dark halos might be better tracers of the observed galaxies than matter, they are still biased tracers. We address this problem by introducing the Halo Occupation Distribution (HOD) prescription to locate ‘galaxies’ within our dark halos. We adopt the following recipe of Zehavi et al. (2004). A central galaxy is assigned to a halo if its mass  $M$  exceeds  $M_{\text{min}}$ , and the central galaxy can have satellites. The mean number of satellite galaxies is given by a power-law  $\langle N_{\text{sat}} \rangle = (M/M_1)^\alpha$ , and they have a Poisson distribution. We use, as a toy model, the HOD parameters of  $\log M_{\text{min}} = 11.76$ ,  $\log M_1 = 13.15$ , and  $\alpha = 1.13$  given by Table 3 of Zehavi et al. corresponding to galaxies with an absolute  $r$  magnitude cut of  $M_r = -19.5$  in the Sloan Digital Sky Survey. These ‘galaxy’ tracers are used in subsection 5.3.

As an another galaxy formation model we adopt the biased galaxy formation scenario where galaxies form at peaks in the initial density field (Bardeen et al. 1986). We use PM simulations of  $1024^3$  CDM particles in a  $2048^3$  mesh spanning  $409.6h^{-1}$  Mpc along a side. In the  $\Lambda$ CDM model a set of peak bias parameters,  $\nu_{\text{th}} = 0.05$  and  $R_s = 0.763h^{-1}$  Mpc, gives us peak particles which cluster like bright galaxies at the present epoch, where  $\nu_{\text{th}}$  is the threshold density level for the peaks, and  $R_s$  is the Gaussian smoothing length corresponding to the galaxy scale. In the case of the SCDM model, the peak parameters adopted are  $\nu_{\text{th}} = 1.7$  and  $R_s = 0.585h^{-1}$  Mpc for  $\sigma_{\text{mass},8} = 0.6$ . These peak particles have been shown to follow the centers of collapsed dark halos, but are too clustered in high density regions since no merging process is included (Park & Gott 1991).

#### 5. RESULTS

We have measured the genus statistics in the four dimensional space of smoothing scale, redshift, tracers, and cosmogony. We use Gaussian smoothing and the defini-

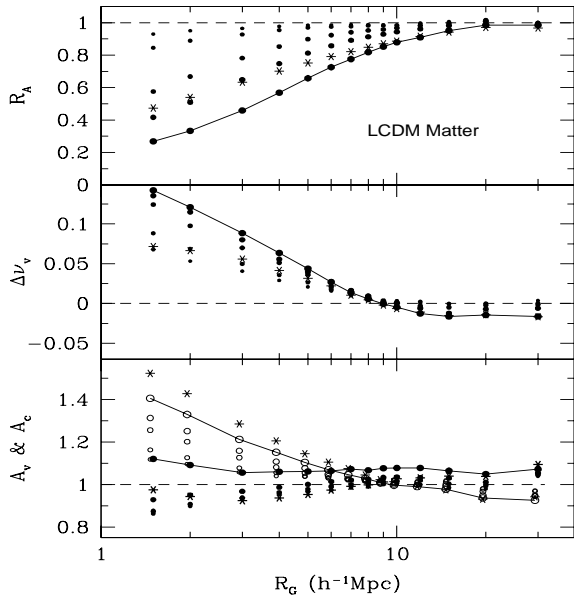


FIG. 1.— The genus-related statistics for dark matter measured from the LCDM1024 simulation. Dots with different sizes represent the statistics at redshifts  $z = 0, 1, 2, 5,$  and  $8$ . The largest dots connected by lines are for  $z = 0$ , and the smallest are for  $z = 8$ . In the bottom panel filled circles are  $A_C$ 's, and open circles are  $A_V$ 's which are slightly shifted to avoid confusion. Stars are the statistics measured in redshift space. In the bottom panel bold stars are  $A_C$ 's, and thin stars are  $A_V$ 's.

tion of the smoothing length  $R_G$  is standard ( $\sqrt{2}$  times larger than the ‘e-folding’ smoothing adopted by Gott et al. (1989)). We always maintain the condition that the Gaussian smoothing length  $R_G$  must be greater than or equal to the mean particle/halo separations. Topology is explored at 14 smoothing scales from  $R_G = 1.5h^{-1}$  Mpc to  $30h^{-1}$  Mpc in the case of the matter distribution. Our large and high resolution simulations enable us to obtain very accurate genus values. The number of resolution elements in the simulation box is over  $2500 (= L^3/(2\pi)^{3/2}R_G^3)$  at the largest smoothing scale  $R_G = 30h^{-1}$  Mpc, and exceeds  $2 \times 10^7$  at  $R_G = 1.5h^{-1}$  Mpc. The genus is also calculated at 7 epochs with redshifts  $z$  from 0 to 8, but we show results only at  $z = 0, 1, 2, 5,$  and  $8$  to avoid over-crowding of points in figures.

### 5.1. $\Lambda$ CDM Dark Matter

The mean particle separation of the LCDM1024 simulation is  $0.5h^{-1}$  Mpc, and we explore the topology of the dark matter distribution from  $R_G = 1.5h^{-1}$  to  $30h^{-1}$  Mpc. The size of density array is  $2048^3$ , so the smoothing length is at least three times larger than the pixel size (thus avoiding discreteness effects). The results for the genus-related statistics are shown in Figure 1 as filled and open circles. Dots with different sizes represents the statistics at different redshifts from  $z = 0$  (largest circles connected by solid lines), 1, 2, 5 to 8 (smallest). The dark matter in the  $\Lambda$ CDM universe clearly shows an intriguing development of small-scale topology in the cases of  $\Delta\nu$  and  $A_V$  statistics in a direction opposite to that at large scales. The shift parameter  $\Delta\nu$  rapidly goes to positive values at  $R_G < 9h^{-1}$  Mpc. But at scales  $R_G > 9h^{-1}$

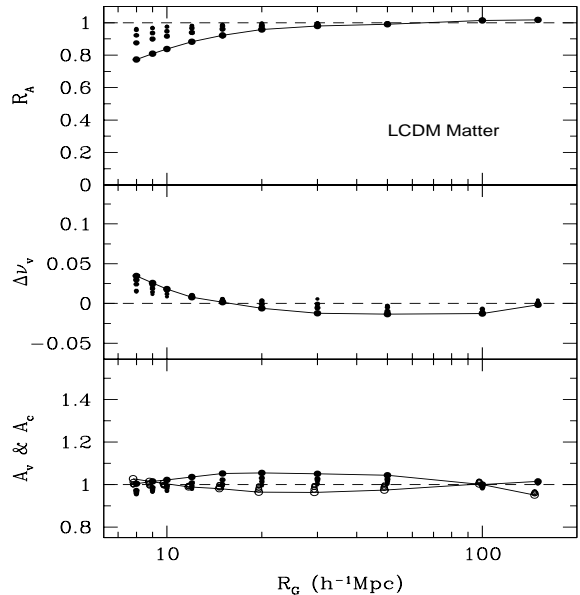


FIG. 2.— Same as Figure 1, but statistics are calculated from the LCDM5632 simulation. Note that the data at  $z = 8$  and  $5$  are almost overlapping. Only measurements in real space are plotted.

Mpc it slowly moves in the negative direction and continues to be negative even at  $30h^{-1}$  Mpc scale. All these genus curves have a spongelike topology ( $G > 0$ ) at the median density contour, so we would not call the negative and positive shifts of the central part of the genus curve as in the direction of ‘meat-ball’ and ‘bubble’ topologies, respectively, since their correspondence does not seem to be so simple. The transition scale of  $\Delta\nu$  from positive to negative shift agrees with the analytic prediction of subsection 5.6.

In Figure 2 the genus-related statistics calculated from the LCDM5632 simulation are plotted to show their behaviour at larger scales. Note that the power spectrum of LCDM5632 is slightly different from that of LCDM1024, thus making the transition scale of  $\Delta\nu$  occur at different  $R_G$ . It can be seen that non-Gaussianity is visible up to the scale  $\sim 100h^{-1}$ Mpc. But using the analytic estimation of the non-Gaussianity effects of gravitational evolution in this weakly non-linear scales given in subsection 5.6, one could draw conclusions on the Gaussianity of the initial density field from data with smoothing lengths much smaller than  $100h^{-1}$ Mpc if the matter distribution can be used.

The parameter  $A_V$  for voids (open circles in the bottom panels of Figure 1 and 2) shows a behaviour similar to the shift parameter. At scales below  $10h^{-1}$  Mpc voids are broken into many pieces and the number of voids exceeds the Gaussian value predicted by the middle part of the genus curve (see Figure 1). But at larger scales voids percolate and the number of voids is slightly less than the Gaussian value (see Figure 2). On the other hand, the parameter  $A_C$  for clusters (filled circles in the bottom panel of Figure 1 and 2) behaves differently. It tends to increase at all scales at the present epoch. The speed with which new high density clumps stick up above the threshold and appear in the sample is faster than that of merging and disappearance of existing clumps. But at

very small scales ( $R_G \leq 2h^{-1}$  Mpc) the merging speed wins over the sticking-up speed at high redshifts ( $z \geq 5$ ) and subsequently the situation reverses. At large scales, the sticking-up of clusters and merging of voids are the dominant processes (Figure 2). It should be noted that gravitational evolution only makes the both parameters  $A_V$  and  $A_C$  increase over 1 at scales below  $10 h^{-1}$  Mpc at the present epoch. Therefore, the observed value of the void abundance parameter  $A_V$  which is less than 1 (Park et al. 2005) must be due to strong biasing effects, which tend to make small voids merge with one another. This can be achieved if galaxies do not form in weak walls and filaments of large scale structure dividing small voids.

The amplitude drop parameter shown in the top panel of Figure 1 evolves very rapidly at scales below about  $10 h^{-1}$  Mpc as the gravitational evolution proceeds. And its scale dependence is again determined by the characteristic shape of the power spectrum of the  $\Lambda$ CDM model.

Also shown in the figures are the genus-related statistics measured in redshift space at  $z = 0$  (stars in all figures). We adopt the far-field approximation to the redshift distortion of the density field. Displacement of particles is thus assumed to occur only along the direction of a coordinate axis. We average three genus curves measured from redshift space density fields each of which is perturbed in the direction of each coordinate axis using the periodic boundary condition. Genus and the power spectrum of density field in redshift space are measured to calculate the genus-related statistics. The amplitude drop parameter  $R_A$  increases in redshift space because the amplitude of the random-phase genus curve ( $A_{PS}$  in Equation (7)) drops more than that of non-linear genus curve ( $A_{obs}$ ) due to the randomization effects of small-scale peculiar velocity. Effects of redshift space distortions on the genus curve have been previously studied by Melott, Weinberg, & Gott (1988). They have reported that the effects are negligible when a smoothing larger than the correlation length is applied to the density field. And the linear regime calculation of Matsubara (1996) has supported their claim. Subsequently, redshift space distortion effects have been generally ignored in the genus analyses. This is qualitatively true for the matter field of the  $\Lambda$ CDM model where the correlation length is about  $5.5 h^{-1}$  Mpc at  $z = 0$  and smoothing lengths larger than this are studied. However, as can be seen in our figures, there are non-negligible systematic effects of redshift space distortion on the genus related statistics at the small smoothing scales we are interested in. An example is the  $A_C$  parameter (thick stars in the bottom panel of Figure 1). Being a measure of the topology of high density regions,  $A_C$  is most sensitive to the peculiar velocity field.

### 5.2. $\Lambda$ CDM Biased Peak Particles

We use the peaks in the initial Gaussian density field as the biased ‘galaxy’ particles. They are defined by the threshold level  $\nu_{th}$  and the galaxy scale  $R_s$  (Park & Gott 1991), which are chosen so that the resulting biased particles approximate the distribution of galaxies at the present epoch. When we require them to have  $\sigma_{pk,8} = 1$  and to have a correlation function close to the observed galaxy CF at  $z = 0$ , we find a set,  $\nu_{th} = 0.05$  and  $R_s = 0.763h^{-1}$  Mpc in our  $\Lambda$ CDM universe with  $\sigma_{m,8} = 0.9$ . The number density of the peaks is much

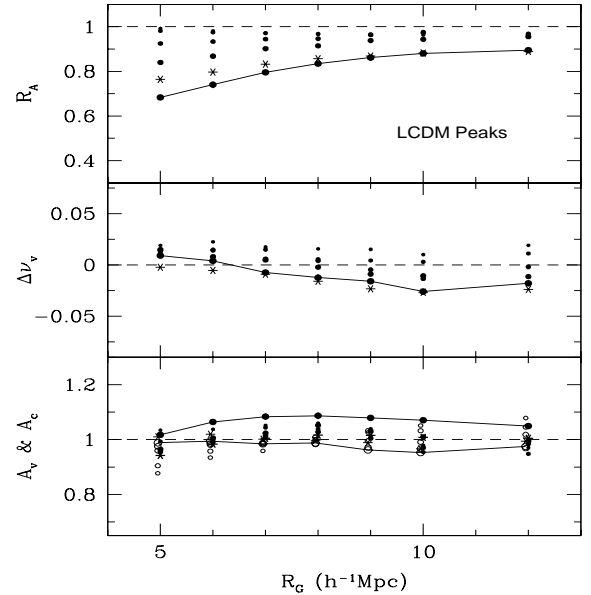


FIG. 3.— Genus-related statistics for the biased peaks calculated from the  $\Lambda$ CDM410 simulation. Notations are the same as Figure 1.

lower than that of CDM particles, and the genus is measured only at scales  $R_G \geq 5h^{-1}$  Mpc. The simulation used for identifying the biased peak particles is the  $\Lambda$ CDM model evolved by the PM code in a  $2048^3$  mesh spanning  $409.6h^{-1}$  Mpc along a side. Its small pixel size ( $0.2h^{-1}$  Mpc) allows us to look for density peaks at the galaxy scale  $R_s$ . The genus-related statistics of the biased peak particles are shown in Figure 3. Even though our biased density peaks collapse at a specific epoch and can be considered as galaxies after then, we plot the statistics of the biased particles at all epochs after  $z = 8$  for theoretical interest.

They behave essentially in the same way as those for cold dark matter, but there are some changes. Similarly to before, the peak particles develop a negative shift  $\Delta\nu$  at scales larger than  $6h^{-1}$  Mpc, and a positive shift at smaller scales. And the cluster abundance parameter  $A_C$  increases at all scales above  $5h^{-1}$  Mpc. However, the void abundance parameter  $A_V$  (open circles in Figure 3) shows more changes. Namely, at scales smaller than about  $7 h^{-1}$  Mpc the biasing prescription makes small voids percolate and  $A_V$  become less than 1 at high redshifts. As noted above, gravitational evolution only makes  $A_V$  increase above 1 at scales less than  $10 h^{-1}$  Mpc, contrary to observations. Here we have a specific example of a galaxy formation mechanism which allows existing voids to percolate strongly enough to overcome the nonlinear gravitational effect of opening of new voids and makes  $A_V$  less than 1.

The stars in Figure 3 are the statistics measured in redshift space at  $z = 0$ . The effect significantly decreases  $A_C$  (bold stars in the bottom panel of Figure 3) at all scales explored as dense clusters are spread along fingers-of-god. It can be noted that the void abundance parameter is not much affected by the redshift space distortion because empty regions are much more stable to the distortion compared to dense clumps. This observation is also true for other tracers used in this work. Given its

insensitivity to redshift space distortion,  $A_V$  is a crucial statistic telling the story of galaxy formation in a less distorted way.

### 5.3. $\Lambda$ CDM Dark Halos

The biased particles studied above are the density peaks in the Gaussian initial density field. This structure formation scheme assumes that galaxies form at the maxima in the primordial density fluctuations. It can be shown that these actually correspond well to collapsed dark halos at the final epoch of simulations (Park & Gott 1991). However, it would be good to check the idea and to re-compute the same statistics by using physically bound dark halos identified in high resolution simulations. Another important difference between the biased peak particles and dark halos is that formation of tracers is naturally incorporated in the genus analysis in the case of dark halos. Since we need high resolution for halo formation and identification and large volume for high statistical significance, the LCDM1024 simulation is used. The minimum halo mass identified is  $5 \times 10^{11} M_\odot$  (53 particles). With the dark halo samples obtained from this simulation, topology of the dark halo distribution is studied at scales from 5 to 30  $h^{-1}$  Mpc at  $z = 0$ . At higher redshifts the minimum smoothing length used becomes larger as the dark halos collapsed by then become rarer.

The genus-related statistics measured for the dark halos in the  $\Lambda$ CDM model are shown in Figure 4. Topology of  $\Lambda$ CDM dark halos is very different from those of underlying dark matter or biased peak particles. The shift parameter  $\Delta\nu$  starts from large negative values at high redshifts when the only densest regions can collapse. Consistent with this behaviour the  $A_C$  parameter is greater than 1, and  $A_V$  is lesser than 1 at high redshifts. At lower redshifts, the topology of the dark halo distribution evolves strongly.  $\Delta\nu$  becomes positive and  $A_C$  becomes less than 1. This is opposite to what we have seen in the case of CDM matter and biased peak particle distributions.  $A_V$  still stays below 1 but has increased from its high redshift value, which is consistent with the case of biased peak particles.  $A_C$  of dark halos rapidly decreases at low redshift while that of peak particles keeps increasing. This is because the dark subhalos merge to form one huge halo at centers of clusters of halos, and thus decreasing the number of subhalos or reducing the richness of clusters as non-linear evolution proceeds at small scales. This merging process within clusters does not exist for peak particles because peak particles never lose their identity and the clusters of peak particles get richer as they become more compact. The reality might be somewhere between these two extremes. Comparison of Figure 4 with previous ones demonstrates sensitivity of the topology to the galaxy formation mechanism. Since galaxies show different topology depending on their internal physical properties, topology analysis can be used to discriminate among different galaxy formation mechanisms for different species of galaxies.

Hikage, Taruya & Suto (2003) have calculated the biasing and genus of dark matter halos as a function of halo mass and smoothing scale by using the Hubble Volume Simulation. They have found that the halo biasing effects on the genus are comparable to the non-Gaussianity due to the non-linear gravitational evolu-

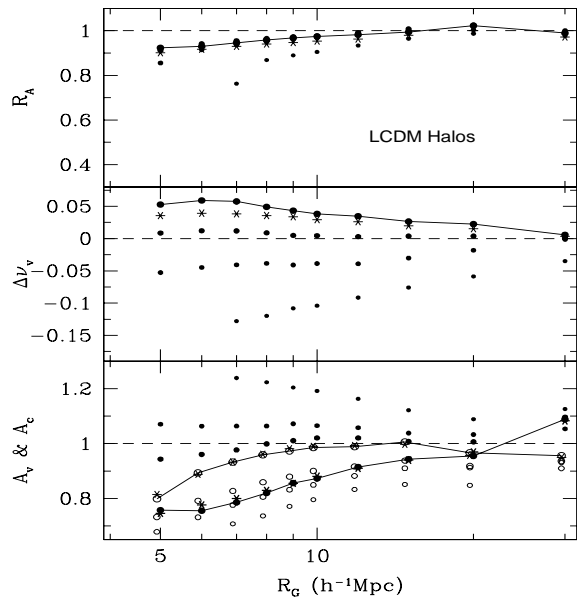


FIG. 4.— Genus-related statistics for the dark halos calculated from the LCDM1024 simulation. Notations are the same as Figure 1. Since the number density of dark halos at  $z = 8$  and 5 is too low, we show the results at  $z = 0, 1, 2$ , and 3.5. And at  $z = 3.5$  (smallest points) genus is measured at  $R_G \geq 7h^{-1}$  Mpc.

tion. This is consistent with our results that changes of the genus-related statistics due to gravitational evolution at  $R_G = 30h^{-1}$  Mpc scale is of the order of that due to tracer difference. Hikage et al. (2003) have studied topology of halo distribution at  $R_G \geq 30h^{-1}$  Mpc. However, at  $R_G = 30h^{-1}$  Mpc their results are thought to be affected by discreteness effects because the mean separation of their halo subsets is only about  $44h^{-1}$  Mpc. In topology analysis of a set of points, the smoothing length should be larger than the mean tracer separation to avoid systematic discreteness effects, or some correction should be made to remove the effects (Park et al. 2005). The large pixel size of  $23h^{-1}$  Mpc used in their analysis may have also caused some discreteness effects at that smoothing scale. In general one wants the smoothing length  $R_G$  to be at least 1.77 times the pixel size to avoid discreteness effects (eg. Hamilton, Gott, & Weinberg 1986). To identify halos they have used the friends-of-friends algorithm, which is known to miss subhalos within big halos and often produces unphysical halos connected by narrow chains of particles. Therefore, it is not easy to directly compare their results with those of the current work in detail. But our results qualitatively agree with their conclusion that non-Gaussianity induced by halo biasing is comparable to that by the non-linear gravitational evolution.

### 5.4. HOD Galaxies

A halo identified in the N-body simulation might not contain a galaxy, or can host more than one galaxies. Therefore, even though dark halos might be a better tracer of the observed galaxies than matter, they may not be representing galaxy distribution well enough to allow quantitative comparisons. We address this problem by introducing the Halo Occupation Distribution (HOD) prescription to locate ‘galaxies’ within our dark

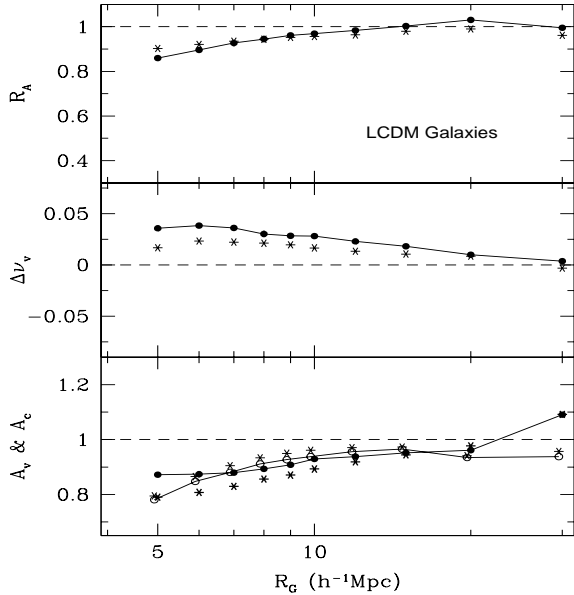


FIG. 5.— Genus-related statistics for the ‘galaxies’ derived from the dark halos of the LCDM1024 simulation. Notations are the same as Figure 1. Only the results at  $z = 0$  are shown.

halos. We adopt the following recipe of Zehavi et al. (2004). A central galaxy is assigned to a halo if its mass  $M$  exceeds  $M_{\min}$ , and the central galaxy can have satellites. The mean number of satellite galaxies is given by a power-law  $\langle N_{\text{sat}} \rangle = (M/M_1)^\alpha$ , and they have a Poisson distribution. The satellites are randomly located at distances of  $0.3h^{-1}\text{Mpc}$  from the central galaxy. This does not change our results because the minimum smoothing scale adopted for analysis of the HOD galaxies is  $5h^{-1}\text{Mpc}$ . We use, as a toy model, the HOD parameters of  $\log M_{\min} = 11.76$ ,  $\log M_1 = 13.15$ , and  $\alpha = 1.13$  given by Table 3 of Zehavi et al. corresponding to galaxies with an absolute  $r$  magnitude cut of  $M_r = -19.5$  in the Sloan Digital Sky Survey.

In Figure 5 we show the genus-related statistics calculated from distribution of ‘galaxies’ assigned within dark halos of the LCDM1024 simulation according to the HOD prescription. The correlation length of these model galaxies is  $5.6h^{-1}\text{Mpc}$ , similar to that of bright optical galaxies. Only the results at  $z = 0$  are shown. Comparing the statistics with those of dark halos at  $z = 0$ , we find  $\Delta\nu$  becomes less positive,  $A_C$  is increased, and  $A_V$  is decreased. These changes the topology of our HOD ‘galaxies’ to be more compatible with that observed for SDSS galaxies (Park et al. 2005). Topology depends on the type of observed galaxies, but one phenomenon consistently found in observations is that the  $A_V$  parameter is less than 1. And This behaviour is seen in the distribution of our HOD ‘galaxies’. However, the observed  $A_C$  parameter is typically greater than  $A_V$ , which does not quite agree with the HOD ‘galaxies’. The HOD method seems to be promising in explaining not only the one-point and two-point functions of galaxy distribution, but also functions of high-order moments like genus. However, more detailed comparisons have to be made to confirm it.

Benson et al. (2001) has used a semi-analytic model

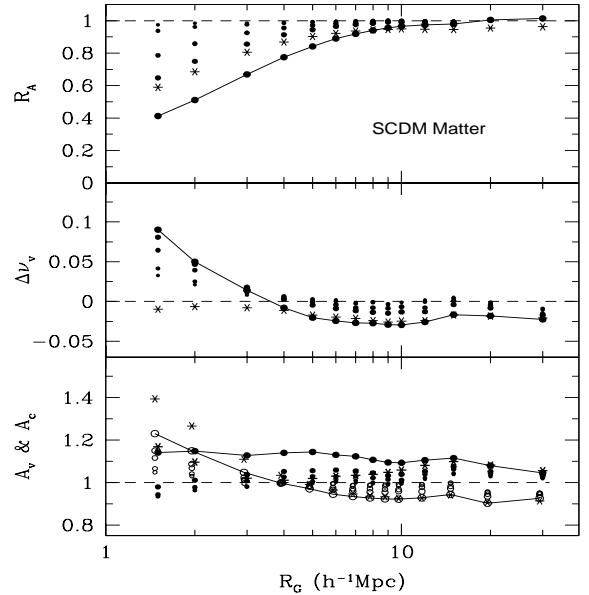


FIG. 6.— Genus-related statistics for dark matter measured from the SCDM1024 simulation. Notations are the same as Figure 1.

of galaxy formation to obtain the distribution of model galaxies, and to measure the genus curves at smoothing lengths of  $4.24$  and  $5.66 h^{-1}\text{Mpc}$  at redshifts  $z = 0$  and  $1$ . But they have not been able to detect the difference between the genus curves for the dark matter and the model galaxies due to sparseness and smallness of their simulation data.

### 5.5. SCDM Case

As a fiducial model we consider the SCDM model to study the dependence of topology on cosmology. In this model  $\Omega_m = 1$  and  $h = 0.5$ , and we adopt a bias factor  $b = 1.5$  and Bardeen et al. (1996)’s fitting formula for the power spectrum. Figure 6 shows that the matter distribution of the SCDM universe has qualitatively the same topology as that of the  $\Lambda\text{CDM}$  universe. Only the characteristic scales are moved down in the cases of  $\Delta\nu$ , and  $A_V$ . The switching from negative to positive shift occurs at  $\sim 4h^{-1}\text{Mpc}$ , and the switching from sub-Gaussian to super-Gaussian amplitude for the void part of the genus curve occurs at a similar scale. This change in the characteristic scales is the direct consequence of the change in the shape of power spectrum. Figure 7 shows the statistics for the biased peak particles found in the SCDM simulation. For  $\Delta\nu$  a negative shift prevails at all scales, and the redshift space distortion effects make little change in  $\Delta\nu$ . Gravitational evolution makes the  $A_C$  parameter increase above 1 as in the  $\Lambda\text{CDM}$  case while the redshift space distortion effects make it decrease. The void abundance parameter  $A_V$  is significantly less 1 due to the biasing effects at small scales, and is hardly affected by the redshift space distortion as in the  $\Lambda\text{CDM}$  case.

### 5.6. Comparison with Perturbation Theory

Matsubara (1994) has obtained a formula for the genus curve modified due to gravitational evolution in the weakly non-linear regime by perturbatively expanding the statistic in  $\sigma_0 = (\delta\rho/\rho)_{\text{rms}}$ , the RMS fluctuation of

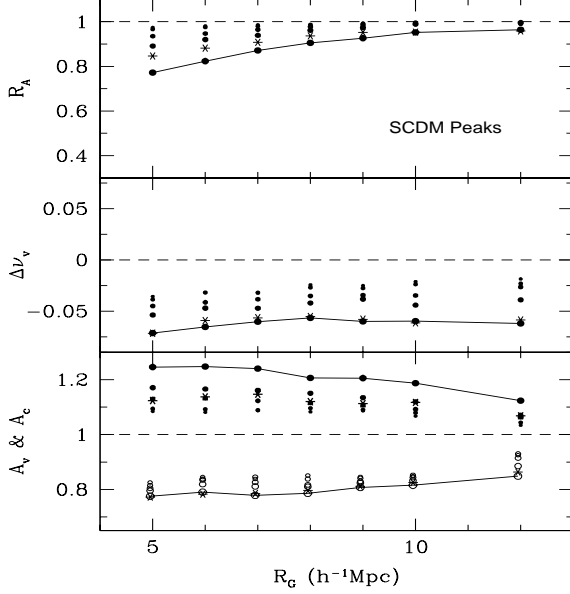


FIG. 7.— Genus-related statistics for the biased peaks measured from in the SCDM410 simulation. Notations are the same as Figure 1.

an over-density field smoothed over a given scale. The non-linear correction in the genus curve to the first order in  $\sigma_0$  is an odd function of  $\nu$  and, therefore, causes a shift and an asymmetry between the high and low density regions. It is hoped that the gravitational evolution effects on genus in the weakly non-linear regime can be modeled by this analytic theory. When the volume threshold level is used, the three-dimensional genus expanded to the first order in  $\sigma_0$  is given by (Matsubara 2003)

$$G(\nu_f) = \frac{1}{(2\pi)^2} \left( \frac{\sigma_1}{\sqrt{3}\sigma_0} \right)^3 e^{-\nu_f^2/2} (1 - \nu_f^2) - [(S^{(1)} - S^{(0)})(\nu_f^3 - 3\nu_f) + (S^{(2)} - S^{(0)})\nu_f] \sigma_0, \quad (9)$$

where the variance parameters are

$$\sigma_j^2(R) = \int \frac{k^2 dk}{2\pi^2} k^{2j} P(k) W^2(kR), \quad (10)$$

and the window function is a Gaussian  $W(kR) = \exp(-k^2 R^2/2)$ .  $S^{(i)}$  are the skewness parameters defined as

$$S^{(0)} = \langle \delta^3 \rangle / \sigma_0^4 = \frac{1}{\sigma_0^4} \int \frac{d^3 k_1}{(2\pi)^3} \frac{d^3 k_2}{(2\pi)^3} B(k_1, k_2, k_{12}), \quad (11)$$

$$S^{(1)} = -\frac{3}{4} \langle \delta^2 \nabla^2 \delta \rangle / \sigma_0^2 \sigma_1^2 = \frac{3}{4\sigma_0^2 \sigma_1^2} \int \frac{d^3 k_1}{(2\pi)^3} \frac{d^3 k_2}{(2\pi)^3} k_{12}^2 B(k_1, k_2, k_{12}), \quad (12)$$

$$S^{(2)} = -\frac{9}{4} \langle (\nabla \delta \cdot \nabla \delta) \nabla^2 \delta \rangle / \sigma_1^4 = \frac{9}{4\sigma_1^4} \int \frac{d^3 k_1}{(2\pi)^3} \frac{d^3 k_2}{(2\pi)^3} \mathbf{k}_1 \cdot \mathbf{k}_2 k_{12}^2 B(k_1, k_2, k_{12}) \quad (13)$$

where  $k_{12} = |\mathbf{k}_1 + \mathbf{k}_2|$  and  $B$  is the bispectrum. The skewness parameters can be calculated from (Matsubara 2003)

$$S^{(0)} = (2 + E)S_0^{11} - 3S_1^{02} + (1 - E)S_2^{11}, \quad (14)$$

$$S^{(1)} = \frac{3}{2} \left( \frac{5 + 2E}{3} S_0^{13} - \frac{9 + E}{5} S_1^{22} - S_1^{04} + \frac{2(2 - E)}{3} S_2^{13} - \frac{1 - E}{5} S_3^{22} \right), \quad (15)$$

$$S^{(2)} = 9 \left( \frac{3 + 2E}{15} S_0^{33} - \frac{1}{5} S_1^{24} - \frac{3 + 4E}{21} S_2^{33} + \frac{1}{5} S_3^{24} - \frac{2(1 - E)}{35} S_4^{33} \right), \quad (16)$$

where

$$E \approx \frac{3}{7} \Omega_m^{-1/30} - \frac{\Omega_\Lambda}{80} \left( 1 - \frac{3}{2} \Omega_\Lambda \log_{10} \Omega_m \right), \quad (17)$$

and

$$S_m^{\alpha\beta} = \frac{\sqrt{2\pi}}{\sigma_0^4} \left( \frac{\sigma_0}{\sigma_1 R} \right)^{\alpha+\beta-2} \int \frac{\ell_1^2 d\ell_1}{2\pi^2 R^3} \frac{\ell_2^2 d\ell_2}{2\pi^2 R^3} P\left(\frac{\ell_1}{R}\right) P\left(\frac{\ell_2}{R}\right) \times e^{-\ell_1^2 - \ell_2^2} \ell_1^{\alpha-3/2} \ell_2^{\beta-3/2} I_{m+\frac{1}{2}}(\ell_1 \ell_2). \quad (18)$$

Here  $P$  is the linear power spectrum and  $I_\nu$  are the modified Bessel functions.

We have performed the above integrals to get the skewness parameters for our  $\Lambda$ CDM and SCDM models as a function of smoothing length  $R_G$ . The curves in Figure 8 show the genus-related statistics predicted by equation (9) for the  $\Lambda$ CDM and SCDM models at the present epoch  $z = 0$ . In the top panel the RMS density fluctuation  $\sigma_0$  and the skewness parameters are shown. The differences between the skewness parameters in equation (9) are very small as can be seen here, and make the genus as a function of  $\nu_f$  rather insensitive to gravitational evolution. According to the perturbation theory the amplitude of the genus curve remains the same in the weakly non-linear regime. This is certainly not true because the density field starts to build phase correlations and the genus amplitude starts to decrease as soon as the gravitational evolution occurs. The behaviours of the  $\Delta\nu$ ,  $A_C$ , and  $A_V$  parameters predicted by equation (9) are remarkably similar to those seen in Figure 1 and 6. This is an important confirmation of the Matsubara's theory. The one major failure of the analytic prediction is for the  $A_C$  parameter at small non-linear scales. At high redshifts  $A_C$  decreases below 1 as high density clumps merge together as predicted by the analytic theory. But at lower redshifts  $A_C$  increases to become greater than 1 as the merging rate slows down and the speed new clumps appear becomes higher.

Matsubara (1996) has derived the genus in redshift space in the linear regime. The genus in redshift space predicted by the linear theory is

$$G^{(s)}(\nu) = \frac{3\sqrt{3}}{2} \sqrt{C} (1 - C) G^{(r)}(\nu), \quad (19)$$

where  $G^{(r)}(\nu)$  is the genus curve in real space,

$$C = \frac{1}{3} \left( 1 + \frac{6f}{5b} + \frac{3}{7} \left( \frac{f}{b} \right)^2 \right) / \left( 1 + \frac{2f}{3b} + \frac{1}{5} \left( \frac{f}{b} \right)^2 \right), \quad (20)$$



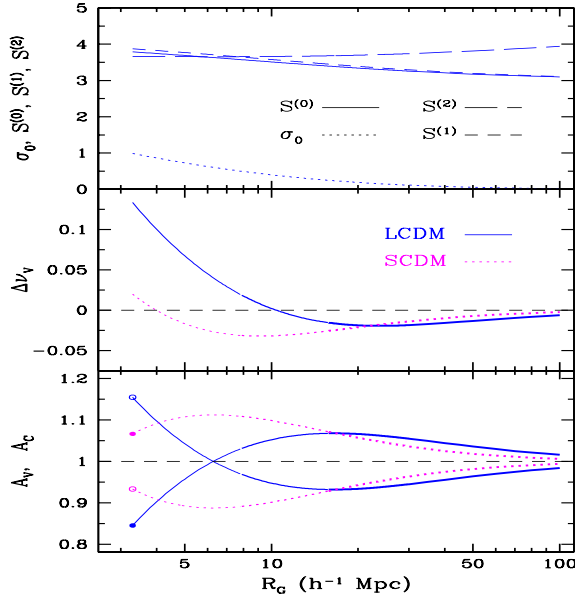


FIG. 8.— Genus-related statistics at  $z = 0$  according to the Matsubara’s perturbation theory. In the second and third panels thick curves are for scales with  $\sigma_0 < 0.25$ , medium thickness curves for  $0.25 \leq \sigma_0 < 0.5$ , and thin curves for  $0.5 \leq \sigma_0 < 1.0$ . In the top panel the RMS deviation of density fluctuation and skewness parameters are plotted.

$b$  is the bias factor, and

$$f = \frac{d \ln D}{d \ln a} \approx \Omega_m^{0.6} + \frac{\Omega_\Lambda}{70} \left(1 + \frac{\Omega_m}{2}\right), \quad (21)$$

where  $D$  is the linear growth factor, and  $a$  is the expansion parameter. The formula says the redshift space distortion does not alter the shape of the genus curve and only affects its amplitude. For matter in our  $\Lambda$ CDM model  $b = 0.9$ ,  $f = 0.468$  and  $C = 0.414$ , and the amplitude drops by a factor of 0.980 while in the SCDM model which has  $b = 1.5$ ,  $f = 1$ , and  $C = 0.433$  the factor is 0.970. In the linear regime the genus amplitude calculated from redshift space power spectrum is equal to that from real space power spectrum since the shape of power spectrum remains the same. This makes the denominator of the amplitude drop parameter  $R_A$  unchanged in redshift space, and makes  $R_A$  itself decrease by above factors in the  $\Lambda$ CDM and SCDM models. This can be observed in Figures 1 and 6 at scales  $R_G \geq 20 h^{-1} \text{Mpc}$ .

Matsubara & Suto (1996) have used N-body simulations to examine the redshift space distortion effects on genus. They have reported that the amplitude of the genus curve is suppressed more than that expected by linear theory, but that its shape in redshift space still remains the same down to weakly non-linear scales. We have also shown that the redshift space distortion effects on the genus curve are small in the linear and quasi-linear scales. But it should be pointed out that the high threshold part of the genus curve (namely the  $A_C$  parameter) is more affected.

Comparisons of numerically calculated genus with theoretical predictions are useful. But so far theories have mainly concerned themselves with the development of non-Gaussianity in the local density field rather than changes in topology. Our genus meta-statistics are directly addressing questions about the gravitational evo-

lution of topology and the effects of biasing and redshift space distortion on topology.

## 6. CONCLUSIONS

We have studied dependence of the genus statistic on cosmology, tracer, redshift, and Gaussian smoothing scale. We summarize our findings.

1. The shift parameter  $\Delta\nu$  of the genus curve shows a strong scale dependence whose characteristics are determined by the shape of the initial power spectrum. For the matter distribution in the  $\Lambda$ CDM model the negative-to-positive transition occurs at  $\sim 9 h^{-1} \text{Mpc}$  while it is at about  $4 h^{-1} \text{Mpc}$  for SCDM. Below these scales gravitational evolution causes strong positive shifts starting from high redshifts. At larger scales the gravitational evolution produces weak negative shifts. This trend enhances as the evolution proceeds. When the topology tracers are biased peak particles instead of CDM particles, evolution of the genus curve is qualitatively similar. But the positive-to-negative transition scale is different, and at small scales  $\Delta\nu$  keeps slowly decreasing, which is opposite to the case of CDM matter particles. We have demonstrated that galaxies can have a topology very different from that of matter on small scales. The  $\Delta\nu$  parameter measured from the dark halo and HOD ‘galaxy’ distributions is positive at scales between 5 and  $30 h^{-1} \text{Mpc}$ , and becomes more positive due to the combined effects of formation of new objects and gravitational clustering. This trend is opposite to that seen in distributions of matter and biased peak particles at scales larger than  $9 h^{-1} \text{Mpc}$ . It remains to be seen which value of the shift parameter the distribution of real galaxies has. The redshift space distortion systematically decreases  $\Delta\nu$  in the  $\Lambda$ CDM universe, and the effects are significant at scales  $\leq 5 h^{-1} \text{Mpc}$ . We can in principle correct for these redshift space distortion effects on  $\Delta\nu$  by using the observationally measured line-of-sight velocity dispersion to correct the shift parameter at both large and small scales for the study of primordial density field and galaxy formation mechanisms.

2. The amplitude drop parameter is more difficult to measure than the genus curve alone because it requires additional accurate measurement of power spectrum for each tracer of topology. Direct consequence of genus amplitude drop is the phase correlation of density field, and the phase correlation depends on the shape of the initial density power spectrum and the biasing. We have found that the dark halos and the HOD ‘galaxies’ show a very small genus amplitude drop with  $0.9 \leq R_A \leq 1$  down to the scale  $5 h^{-1} \text{Mpc}$  with little scale dependence. And it hardly changes due to gravitational evolution or peculiar motions. This might be incompatible with the observationally measured value of about 0.6 at  $5 h^{-1} \text{Mpc}$  for the IRAS Point Source Catalogue Redshift Survey (Canavezes et al. 1988) or for the Center for Astrophysics Survey (Vogeley et al. 1994). Satisfying the constraint from the genus amplitude drop can be a challenge for HOD modeling of galaxy formation.

3. The void abundance parameter  $A_V$  of the dark matter distribution strongly increases above the Gaussian value below  $10 h^{-1} \text{Mpc}$ , but gently drops below 1 at larger scales as the gravitational evolution proceeds. This is true for both  $\Lambda$ CDM and SCDM models even though their transition scales are different. While grav-

itational evolution always raises  $A_V$  at small scales, biasing can lower it below 1 as can be seen for the biased peak particles, dark halos, and HOD ‘galaxies’. Even the direction of evolution of  $A_V$  (and  $A_C$ ) can be changed by biasing. Since  $A_V$  is observed to be less than 1 for the SDSS galaxies (Park et al. 2005), this fact is strong evidence for the existence of biasing in the distribution of galaxies with respect to matter. Fortunately,  $A_V$  at small scales is hardly affected by the redshift distortion effects, and can give faithful constraints on galaxy formation in under-dense regions.

We have considered only three mechanisms for galaxy formation. The peak biasing scheme is able to explain the stronger clustering amplitude for rarer objects (Kaiser 1984). But we have considered only one version of the peak biasing scheme where the threshold for galaxies is a step function, and have not taken into account merging (cf. Narayanan, Berlind, & Weinberg 2000 for various biasing models). The first assumption will affect the voids, and the second the clusters. The arbitrariness of the threshold function can be removed by using the dark halos which have collapsed and are self-bound physical objects. But the dark halos also cannot fully trace galaxies because the mass function of dark halos continuously extends up to supercluster scales and does not show a natural cutoff for galaxies. Some of them with small masses may have lost baryons in high density environments, and have not been able to form stars. The HOD ‘galaxies’ seem to approximate the distribution of real galaxies better than the dark halos because the  $A_V$  parameter is closer to observations for the HOD ‘galaxies’ even though the cluster abundance parameter  $A_C$  may be still too small (cf. Park et al. 2005).

While galaxy formation and evolution in a high density environment are complicated due to the merging of

structures and the high ram pressure of the intergalactic medium (Gunn & Gott 1972), it may be relatively easier to model galaxy formation in low density regions. For example, biased peak particles, dark halos, and HOD ‘galaxies’ all produce  $A_V$  smaller than 1 consistent with observations. But their  $A_C$  are wildly different. Therefore, even though identification of the biased peaks and dark halos with galaxies is not a good approximation in high density regions, they seem to trace galaxies better in under-dense regions for which there is a sensitive measure like the void abundance parameter  $A_V$ . It should be emphasized that the cosmic voids have not been studied as extensively as clusters and superclusters, and it is only in recent years that voids have begun to be actively studied (Hoyle & Vogeley 2004; Sheth & van de Weygaert 2004; Rojas et al. 2004; Colberg et al. 2004). After all, voids are not the places where there is nothing, but places where history of the universe is better kept. With the advent of new large observational data sets like the SDSS sample we can hope better to understand the formation mechanism of each species of galaxies through the topology analysis. We are currently studying the topology of galaxies divided into subgroups with different internal physical properties.

CBP is supported by the Korea Science and Engineering Foundation (KOSEF) through the Astrophysical Research Center for the Structure and Evolution of the Cosmos (ARCSEC) and through the grant R01-2004-000-10520-0. CBP and JHK also acknowledge the support of Korea Institute of Science and Technology Information through the ‘Grand Challenge Support Program’. JRG is supported by NSF grant AST04-06713.

#### REFERENCES

- Benson, A. J., Frenk, C. S., Baugh, C. M., Cole, S., & Lacey, C. G. 2001, MNRAS, 327, 1041  
 Colberg, J. M., Sheth, R. K., Diaferio, A., Gao, L., & Yoshida, N. 2004, astro-ph/0409162  
 Dubinski, J., Kim, J., Park, C., & Humble, R. 2003, New Astronomy, 9, 111  
 Eisenstein, D. J., & Hu, W. 1998, ApJ, 496, 605  
 Gott, J. R. et al. 1989, ApJ, 340, 625  
 Melott, A. L., Weinberg, D. H., & Gott, J. R. 1988, ApJ, 328, 50  
 Gott, J. R., Melott, A. L., Dickinson, M. 1986, ApJ, 306, 341  
 Gunn, J. E., & Gott, J. R. 1972, ApJ, 176, 1  
 Hamilton, A. J. S., Gott, J. R., & Weinberg, D. H. 1986, ApJ, 309, 1  
 Hikage, C., Taruya, A., & Suto, Y. 2003, PASJ, 55, 335  
 Hoyle, F., & Vogeley, M. S. 2004, ApJ, 607, 751  
 Kim, J., & Park, C. 2005, in preparation  
 Matsubara, T. 1994, ApJ, 434, L43  
 Matsubara, T. 1996, ApJ, 457, 13  
 Matsubara, T. 2003, ApJ, 584, 1  
 Matsubara, T., & Suto, Y. 1996, ApJ, 460, 51  
 Mecke, K. R., Buchert, T., & Wagner, H. 1994, A&A, 288, 697  
 Narayanan, V. K., Berlind, A. A., & Weinberg, D. H. 2000, ApJ, 528, 1  
 Park, C. 1990, MNRAS, 242, 59P  
 Park, C. 1997, J. Korean Astron. Soc., 30, 191  
 Park, C. & Gott, J. R. 1991, ApJ, 378, 457  
 Park, C., Gott, J. R., & da Costa, L. N. 1992, ApJL, 392, 51  
 Park, C., Choi, Y.-Y., Vogeley, M. S., Gott, J. R., Kim, J., Weinberg, D. H., Hikage, C., Matsubara, T., Park, M.-G., & Suto, Y. 2005, in preparation  
 Rojas, R. R., Vogeley, M. S., Hoyle, F., & Brinkmann, J. 2004, astro-ph/0409074  
 Schmalzing, J., & Buchert, T. 1997, ApJL, 482, L1  
 Sheth, R. K., & van de Weygaert, R. 2004, MNRAS, 350, 517  
 Springel, V. et al. 1998, MNRAS, 298, 1169  
 Vogeley, M. S., Park, C., Geller, M. J., Huchra, J. P., & Gott, J. R. 1994, ApJ, 420, 525